ACS Photonics

pubs.acs.org/journal/apchd5

Article

Organic Light-Emitting Diodes Comprising an Undoped Thermally Activated Delayed Fluorescence Emissive Layer and a Thick Inorganic Perovskite Hole Transport Layer

Michele Forzatti, Vladimir Held, Edoardo Stanzani, David Hall, Dianming Sun, M. Angeles Hernández-Fenollosa, Isaac Brotons-Alcázar, Peter Siffalovic, Sandra Jenatsch, Eli Zysman-Colman, Henk J. Bolink, and Daniel Tordera*

Cite This: *ACS Photonics* 2024, 11, 4151−4160

Read Online

ACCESS | Metrics & More | Article Recommendations | Supporting Information

ABSTRACT: Organic light-emitting diodes (OLEDs) hold potential for next-generation displays and lighting solutions, but current OLED displays rely on the use of scarce metals or fluorescent emitters. Thermally activated delayed fluorescence (TADF) compounds kickstarted a new, promising class of OLEDs as organic TADF emitters do not contain scarce platinoid elements yet remain highly efficient. However, similarly to phosphorescent emitters, their incorporation into devices typically requires complicated doping techniques when vacuum processed. Lowering the mass production costs of high-performing OLEDs using simpler fabrication techniques remains a challenge. Here, we report OLEDs comprising a thermally evaporated $CsPbCl_3$ perovskite transport layer and a TADF-based single-component emitting layer by exploring different approaches to obtain efficient undoped OLEDs, both solution- and vacuum-processed. We first demonstrated the compatibility of the perovskite layer with the solution processing of a TADF dendrimer for host-free, thick emitting layers, with an efficiency of 15 cd A^{-1} well over a luminance of 1000 cd m^{-2}. Then, we employed a TADF small molecule as the emitter and reduced its layer's thickness to the subnanometer regime, while the incorporation of the perovskite increased the required total device thickness. The resulting devices showed a low turn-on voltage of 3.3 V, a high luminance of 11 152 cd m^{-2}, and a high efficiency of 67.6 cd A^{-1}, equaling that of 20 times thicker emissive layers. These findings highlight the versatility of using a perovskite as a transport layer and the potential of combining it with an undoped TADF emitting layer for fabricating simple, cost-effective, and efficient OLEDs.

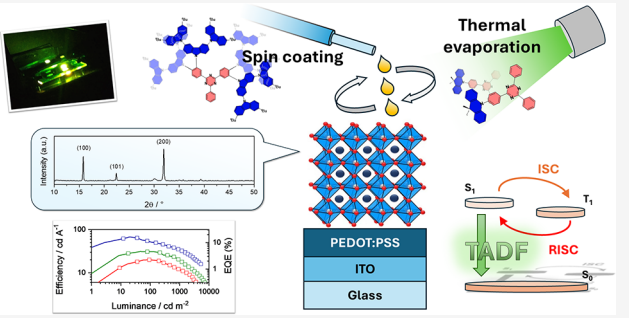

KEYWORDS: *thermally activated delayed fluorescence, organic light-emitting diodes, ultrathin emissive layer, perovskite hole transport layers, vacuum deposition*

Downloaded via UNIV BAYREUTH on November 13, 2024 at 08:26:11 (UTC).
See https://pubs.acs.org/sharingguidelines for options on how to legitimately share published articles.

INTRODUCTION

In recent years, organic light-emitting diodes (OLEDs) have emerged as a leading technology in display and lighting applications, driven by their appealing properties such as their high efficiency, low driving voltage, and fast response, combined with the possibility to manufacture thin and flexible devices.[1,2] In the so-called first-generation OLEDs fluorescent emitters were used, where only singlet excitons (25% of formed excitons) contributed to light emission, while triplet excitons (75%) were lost through nonradiative decay. Phosphorescent emitters containing heavy atoms are used in the current commercial so-called second-generation OLEDs because they can harvest both singlet and triplet excitons by virtue of their strong spin−orbit coupling, allowing for the utilization of up to 100% of the formed excitons. However, they have drawbacks in the form of high materials cost due to the scarcity of the metal elements they contain, toxicity of these elements, and, more importantly, the lack of an efficient and stable blue emitter.[3] Thermally activated delayed fluorescence (TADF) emitters have been proposed as a cost-effective alternative for the fabrication of highly efficient devices as they can convert otherwise nonemissive triplet excitons into emissive singlet excitons when the energy gap between their S_1 and T_1 states is sufficiently small. This process, which is thermally activated, is called reverse intersystem crossing (RISC), and is the mechanism by which both types of excitons are harvested for light emission from the

Received: June 5, 2024
Revised: September 11, 2024
Accepted: September 11, 2024
Published: September 23, 2024

© 2024 American Chemical Society

https://doi.org/10.1021/acsphotonics.4c01039
ACS Photonics 2024, 11, 4151−4160

S_1 state, thus producing devices of comparable efficiency to phosphorescent OLEDs.[4−6]

Most TADF-OLEDs adopt a host−dopant configuration for the emissive layer (EML), which means that the emitting molecules are dispersed in a host material that serves as a matrix.[7−10] While this approach effectively suppresses the unproductive aggregation-caused quenching (ACQ) that arises from the long-lived triplet excitons of the emitter, it complicates device fabrication, and production costs rise as a result. This is especially critical when the devices are prepared by dry processing methods like vacuum deposition, the current industry manufacturing standard, as multiple evaporation sources are used, and precise control is needed in the coevaporation of the different components of the EML. Single-layer OLEDs aim to reduce fabrication costs by minimizing the number of organic compounds and deposition steps.[11] However, they still require simultaneous coevaporation for the emitting layer and offer a more limited selection of host materials. OLEDs featuring nondoped EML offer a simpler and more appealing alternative for mass production, but a careful design of the TADF emitters and/or of the emitting layers is essential to avoid the undesirable ACQ.

As for the design of the TADF emitters, since the rate constant of triplet-related quenching (k_{CQ}) exhibits an exponential dependence on the average intermolecular distance (R), a successful strategy consists in introducing steric hindrance in the molecular structure to enlarge the intermolecular distance.[3] Functional groups with such a property are what the two emitters used in this work, 9′,9″″,9‴‴‴,9⁗⁗⁗-((6-phenyl-1,3,5-triazine-2,4-diyl)bis-(benzene-4,1,2-triyl))tetrakis(3,3″,6,6″-tetra-*tert*-butyl-9′H-9,3′:6′,9″-tercarbazole) (**tBuCz2m2pTRZ**) and 10-(4-(4,6-Diphenyl-1,3,5-triazin-2-yl)phenyl)-9,9-dimethyl-9,10-dihydroacridine (**DMAC-TRZ**), have in common (Figure S1). The former is a TADF dendrimer whose number and distribution of the peripheral *meta*-connected donor dendron moieties have been intentionally devised, among other considerations, so that the density with which they are packed together suppresses the quenching of the emission caused by intermolecular interactions.[12] The latter is a small donor−acceptor (D−A) molecule that contains methyl groups at the sp^3 carbon of the dihydroacridine donor that serve to space the emitter molecules and decrease the interaction between donors. Not only does this emitter display pronounced TADF and high photoluminescence quantum yield, (PLQY) but also it maintains its advantageous characteristics in nondoped films (Figure S2). Not surprisingly, both emitters have indeed been used as a host-free emitting layer in high-efficiency OLEDs, solution-processed in the case of **tBuCz2m2pTRZ** and thermally evaporated in the case of **DMAC-TRZ**.[12,13]

Another strategy to simplify the fabrication process focuses on the design of the layer itself rather than the emitter and consists in reducing its thickness to the subnanometer scale.[14−17] Molecules in such layers (often referred to as "ultrathin") are in the form of isolated domains, making the use of a host unnecessary as the electron (n-type) and hole (p-type) transporting materials on either side of it already fulfill the role of the host. This 2-dimensional counterpart of the usual 3D doping not only simplifies the device manufacturing significantly, but also greatly reduces the materials consumption. However, effective implementation of this approach hinges on two key factors. On one hand, the molecules constituting the ultrathin layer, albeit statistically isolated for the most part, should still possess steric groups to reduce the likelihood of them aggregating in the film. Second, the reduction in the emitting layer thickness should be compensated by thickening the other layers that constitute the device, to prevent shunting paths between the electrodes and the device instability and performance variability that would otherwise result from the reduction in device thickness.[18] A solution to this can be found in the ongoing research effort to use lead-based halide perovskites as charge transport layers in organic and perovskite LEDs,[19−21] since their excellent transport properties (high charge carrier mobility and long diffusion length) allow for an increase in the layer thickness without compromising the efficiency. Indeed, OLEDs with micrometer-scale thick evaporated $CH_3NH_3PbCl_3$ perovskite charge transport layers have been shown to be as efficient as conventional OLEDs,[19] shifting the thickness of the emission layer to the transport layer (while keeping the overall thickness unchanged) without a loss in performance. Such shift is also beneficial from an economical point of view, as perovskite precursors are inexpensive and easily accessible. Even in the case of devices with thicker EMLs, where perovskite hole transport layers (HTLs) do not really play a role in device architecture simplification, they still offer several advantages. First, a thick perovskite HTL can cover dust particles and residues, potentially improving the production yield by minimizing defects that could affect device performance. Additionally, the thick HTL helps smoothing the underlying layer's surface, which is particularly beneficial for solution-processed emitting layers. This smoothing effect reduces the likelihood of filamentary current injection caused by high local electric fields and prevents short-circuits, thereby enhancing device stability and efficiency. Finally, the water-solubility of perovskite materials makes them compatible with a wide range of organic emitters that dissolve in organic solvents, allowing for easy spin-coating and ensuring a uniform, flat surface for subsequent layers.

Despite this, such an approach remains largely unexplored and, to the best of our knowledge, there is no more than a single report of TADF-based OLEDs with thick perovskite transport layers, in which just one TADF emitter was investigated as part of a traditional thermally evaporated thick doped emitting layer. This device showed a maximum EQE (EQE_{max}) of 14%.[19]

In this work, we successfully fabricated OLEDs with a thick (200 nm) fully inorganic cesium lead chloride ($CsPbCl_3$) hole-transporting layer and undoped TADF-based emitting layers, by exploring two approaches for efficient undoped OLEDs. First, devices based on **tBuCz2m2pTRZ**, a TADF dendrimer emitter designed to be used without a need for a host, were prepared by solution processing. An in-depth study of the effect of different solvents on the perovskite transport layer was conducted, showing compatibility between both the perovskite and the emitting layer, and devices were fabricated with efficiencies of 15 cd A^{-1} above 1000 cd m^{-2}. Then, ultrathin devices were prepared using **DMAC-TRZ**, where the thickness of its thermally evaporated layer was optimized to maximize the efficiency. The obtained value of 67.6 cd A^{-1} equals previously reported devices using a nondoped emitting layer but with a significant reduction (∼20×) in materials consumption.

https://doi.org/10.1021/acsphotonics.4c01039
ACS Photonics 2024, 11, 4151−4160

RESULTS AND DISCUSSION

tBucz2m2pTRZ. The high molecular weight of **tBuCz2m2pTRZ** makes it unrealistic to sublime, resulting in the solution-processing of the emitting layer as the only viable option. This generally poses problems in the form of dissolution/disturbance of the underlying hole-transporting layer, which is why, for solution-processed OLEDs, emitting layers are commonly spin-coated directly onto a wet-processed poly(3,4-ethylenedioxythiophene):poly(styrenesulfonate) (PEDOT:PSS) hole injection layer without any additional hole-transporting material. Therefore, in order to use a perovskite hole-transport layer the perovskite needs to be compatible with the solvent used in the emissive layer, as well as be compliant with the optical and electrical requirements of the device. A fully inorganic cesium lead chloride ($CsPbCl_3$) perovskite was selected because of its transparency in the visible range (Figure S3a), its high charge carrier mobility[22] and its ease of fabrication via vacuum coevaporation of its precursors[23] (CsCl and $PbCl_2$), compared to hybrid compositions (like $CH_3NH_3PbCl_3$). Moreover, recent advances in perovskite deposition methods, such as vacuum single-source evaporation, two step vapor-processing, pulsed laser deposition, and solution processing, offer the potential for further simplifying the fabrication process by eliminating the need for coevaporation of precursors.[24−27] Its thickness (200 nm) was chosen to balance a quick deposition time (24 min) with the benefits of thicker transport layers (effective dust coverage, surface smoothing, and reduced short-circuit risk). This value, two times higher than that reached by exceptionally thick organic transport layers,[28] fully emphasizes the unique properties of perovskite HTLs in OLEDs as compared to traditional organic transport materials.

To passivate the interfacial defects, thin CsCl layers (2 nm) are inserted before and after the coevaporated $CsPbCl_3$ layer,[29] enabling sharp photoluminescence and crystallinity (Figure S3b). This stack, CsCl/$CsPbCl_3$/CsCl, will be referred to as modified $CsPbCl_3$ (m-$CsPbCl_3$) for simplicity. As previously stated, the expected little-to-no solubility of chloride perovskite thin films in low polarity organic solvents commonly used in OLED processing (like toluene, chlorobenzene or chloroform) should allow, in principle, for subsequent solution-processing of another layer on top to form multilayered structures.[30]

To verify this, 100-nm thick m-$CsPbCl_3$ films (on top of a PEDOT:PSS CH8000 film) were treated with the three aforementioned solvents by directly spin-coating the solvent on top of the perovskite film (for more details, see the Experimental section). It was noted that the thickness of the layers did not change substantially upon solvent treatment, with a difference of less than 5 nm, compatible with the profilometer uncertainty and film-to-film variations (Table 1).

Table 1. Thickness (Obtained Using a Profilometer) and Root Mean Square Roughness (S_q) (Extracted from the AFM Topographic Images) Values for Thermally Deposited m-$CsPbCl_3$ Thin Films on PEDOT:PSS, Pristine and Treated with Different Solvents[a]

	Pristine	Chloroform	Toluene	Chlorobenzene
Thickness/nm	92	96	92	88
S_q/ nm	5.1	6.5	5.0	5.4

[a]The root mean square roughness calculations were performed on a 25.00 μm^2 projected area.

The bulk properties of the films, namely optical properties such as absorption and photoluminescence spectra, as well as the X-ray diffraction (XRD) patterns were also preserved across the differently treated films (Figure S4).

We also analyzed the solvent effect on the structural properties of the perovskite film by grazing-incidence wide-angle X-ray scattering (GIWAXS). In contrast to conventional Bragg-Brentano geometry, in grazing-incidence geometry the sample is irradiated by an X-ray beam at a small incidence angle, which is not varied during the measurement. In this way, the interaction X-ray path length in the film is increased, the penetration depth into the sample is reduced, and the signal stems primarily from the thin film.[31] Therefore, to investigate the effect of the solvents on the perovskite film surface, it is more insightful to limit the penetration of the X-rays through the substrate and only probe the surface layers. The GIWAXS patterns for the different films, collected with an incident angle of 0.5° and already converted to a q-space, are shown in Figure 1a. First of all, all 2D GIWAXS plots for the m-$CsPbCl_3$ films, pristine and treated with different solvents, appear almost identical, with no significant differences between them. This becomes even more apparent when comparing the normalized azimuthally integrated GIWAXS profiles (Figure 1b), where the overall signal is integrated along the azimuthal angle interval from 0 to 90° (see Figure S5). Moreover, the azimuthal intensity distribution of 100 and 110 Bragg rings at $q \sim 1.1$ $Å^{-1}$ and 1.56 $Å^{-1}$ suggests a preferential orientation of the (100) planes parallel to the substrate. This is also supported by the different relative intensities of the peaks in the XRD patterns for the same films obtained with a conventional Bragg−Brentano X-ray diffractometer (Figure S4c).

Finally, the effect of the solvents on the films' surfaces was also studied by means of atomic force microscopy (AFM). From a visual assessment of the topographic images it was not possible to spot any difference neither in the surface roughness nor in the average grain size (Figure 2, all images colored with the same scale). The visual observations were further confirmed by the calculation of the root-mean-square roughness (S_q) values for each of the films, where a comparable S_q is obtained for each of the films (Table 1, Supporting Information for calculation details). In conclusion, the m-$CsPbCl_3$ film used in this study is compatible with the subsequent solution processing of other layers from a variety of solvents having different polarity, making it a suitable HTL in OLEDs using a solution-processed emitting layer or electron-blocking layer (EBL) on top of the perovskite layer.

Next, devices were fabricated with the following architecture: ITO (150 nm)/PEDOT:PSS CH8000 (40 nm)/m-$CsPbCl_3$ (200 nm)/**tBuCz2m2pTRZ** (40 nm)/PO-T2T (40 nm)/Ba (5 nm)/Ag (70 nm), where ITO and PO-T2T stand for indium tin oxide and 2,4,6-tris[3-(diphenylphosphinyl)-phenyl]-1,3,5-triazine, respectively. The energy level diagram of the device is presented in Figure S6a. The transparent conducting polymer PEDOT:PSS serves as the hole-injection layer. PEDOT:PSS CH8000 was used in place of PEDOT:PSS Al4083 in the final device architecture because it showed better performances in preliminary tests (a 2-fold increase in efficiency, probably because of better charge balance as it reduces hole injection). The emissive layer is composed of a spin-coated neat film of **tBuCz2m2pTRZ**. Given the perovskite layer's compatibility with any nonpolar solvent, chlorobenzene was selected among the tested options due to

https://doi.org/10.1021/acsphotonics.4c01039
ACS Photonics 2024, 11, 4151−4160

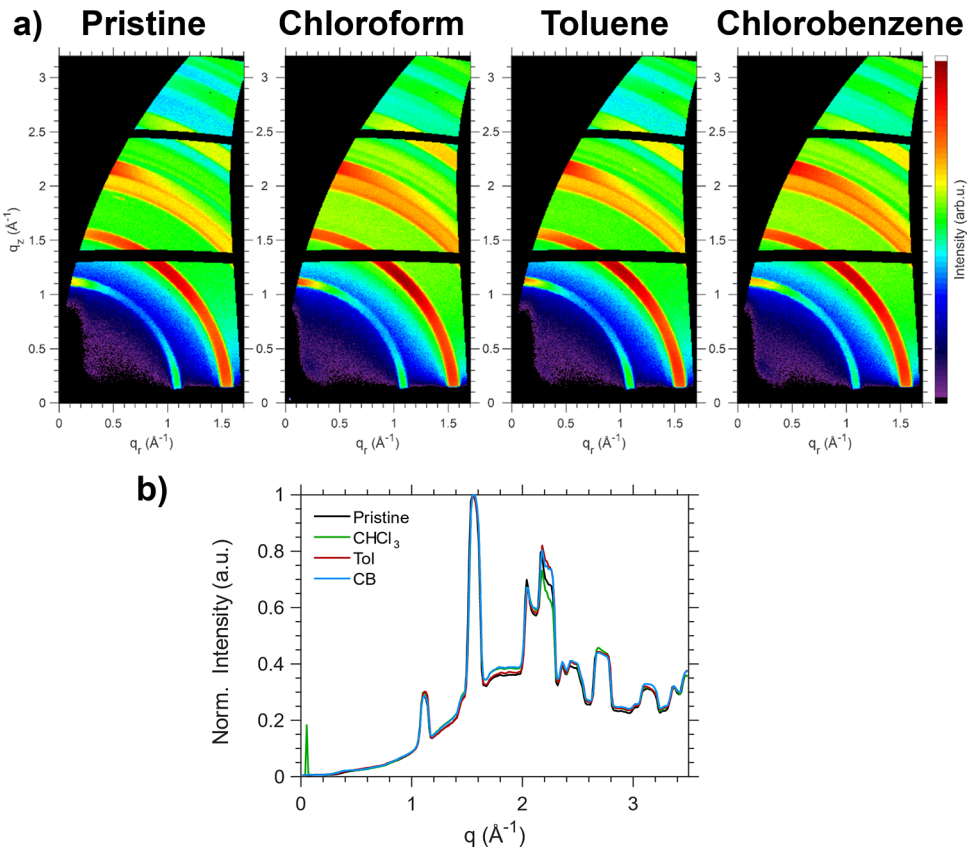

Figure 1. (a) 2D GIWAXS patterns for m-$CsPbCl_3$ films, pristine and treated with different solvents. (b) Normalized azimuthally integrated GIWAXS profiles for the same samples. Tol = toluene, CB = chlorobenzene.

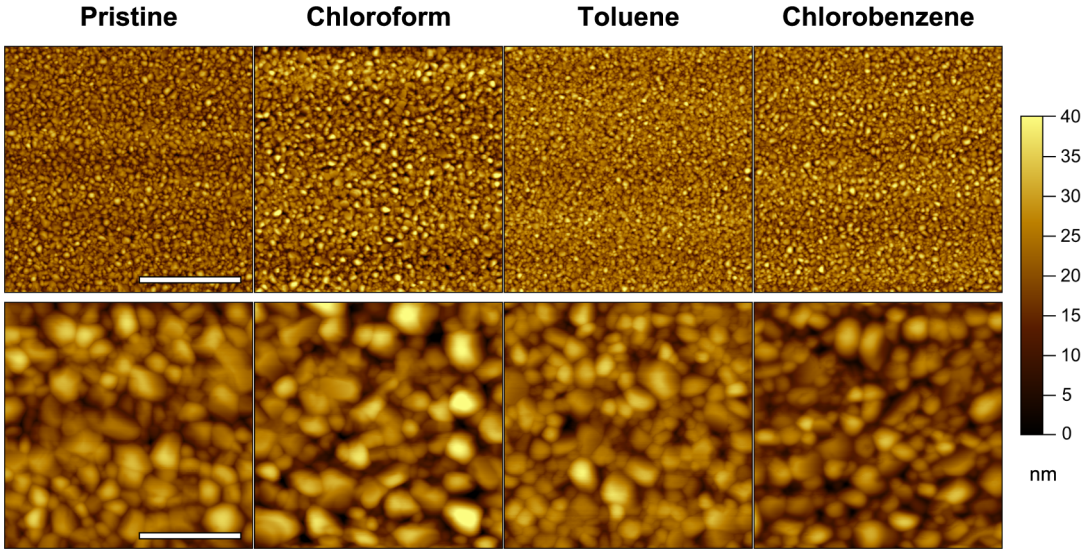

Figure 2. AFM topographic images of a thermally deposited m-$CsPbCl_3$ thin film treated with different solvents. Top row: area = 5 × 5 μm^2, scale bar = 2 μm. Bottom row: area = 1 × 5 μm^2, scale bar = 400 nm.

its prior use in the spin-coating of **tBuCz2m2pTRZ** in high performance solution-processed OLEDs.[12] A cross-sectional SEM image of the entire stack was acquired to gain insight into the perovskite/emitting layer interface (Figure 3a). As expected, the perovskite layer showed no sign of solvent damage and appeared smooth and homogeneously covered by the upper **tBuCz2m2pTRZ** layer.

Figure 3b shows the electroluminescent (EL) spectra as a function of voltage for the devices. Pure green emission (peak at 565 nm, CIE coordinates of 0.46, 0.53) is observed from the TADF dendrimer, suggesting that charge recombination occurs in the undoped emitting layer and that there is efficient hole transport from the perovskite layer to the dendrimer molecules. The emission spectrum is independent of the applied voltage, which means that the CIE color coordinates

https://doi.org/10.1021/acsphotonics.4c01039
ACS Photonics 2024, 11, 4151−4160

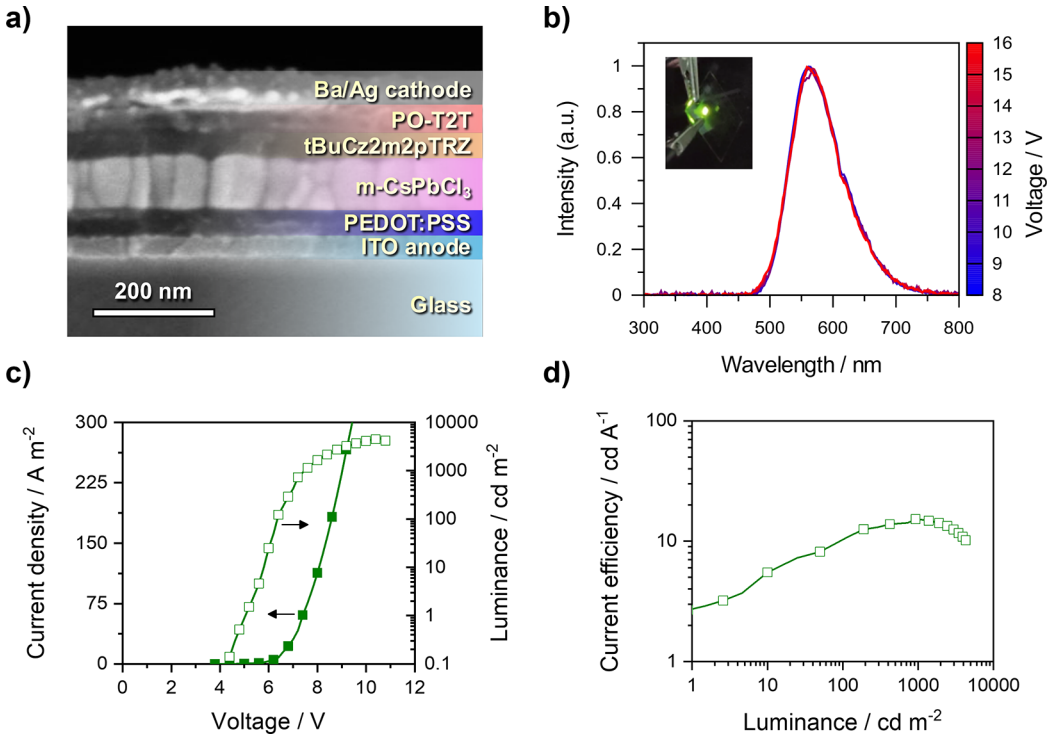

Figure 3. (a) Cross-sectional SEM image of the device stack. (b) Electroluminescence spectrum versus voltage for OLEDs with an m-$CsPbCl_3$ HTL and a solution-processed tBuCz2m2pTRZ (inset: photo of a working device). (c) Current density−voltage−luminance (J−V−L) characteristics and (d) current efficiency versus luminance for the same OLEDs.

also do not change with increasing luminance (Figure S9). Figure 3c,d shows the current density−voltage−luminance (J−V−L) and the current efficiency vs luminance of the devices. The devices reach a peak luminance of 4660 cd m^{-2} (at 10.6 V) with a turn-on voltage (defined as the voltage required to reach a luminance value of 1 cd m^{-2}) of 5.1 V. The current efficiency is above 15 cd A^{-1} at a high luminance of 1000 cd m^{-2}. When compared with a previous report,[12] the peak efficiency of these devices is lower, probably due to a mismatch between the energy levels of the perovskite and the active layer. Indeed, due to the very deep lowest unoccupied molecular orbital (LUMO) of the perovskite when compared to the EML (−3.8 vs −2.8 eV, Figure S6a), electrons might not be properly blocked and confined within the EML, thus decreasing the efficiency.[32] The use of orthogonal solvent systems or cross-linkable materials that can form robust EBLs resistant to subsequent solution processing steps can be explored to address this challenge in future work, while the introduction of PVDF (polyvinylidene fluoride) or PMMA (poly(methyl methacrylate)) interlayers[33] or the mixing of deep HOMO materials with PEDOT:PSS[34] are two possible ways of reducing the hole injection barrier (HIB) with the aim of improving the performance. This is, however, beyond the scope of this work. More importantly, the results highlight that the use of $CsPbCl_3$ as HTL is compatible with solution-processed OLEDs.

DMAC-TRZ. **DMAC-TRZ** is a small molecule that can be processed via thermal evaporation. In order to fabricate devices using a perovskite HTL and an ultrathin **DMAC-TRZ** EML the following architecture was chosen: ITO (150 nm)/PEDOT:PSS Al 4083 (30 nm)/m-$CsPbCl_3$ (200 nm)/mCP (10 nm)/**DMAC-TRZ** (0.1−1 nm)/PO-T2T (60 nm)/Ba (5 nm)/Ag (70 nm), where mCP stands for 1,3-bis(N-carbazolyl)benzene. The energy band diagram of the devices is shown in Figure S6b. The same m-$CsPbCl_3$ (CsCl (2 nm)/$CsPbCl_3$ (200 nm)/CsCl (2 nm)) was used as HTL. mCP and PO-T2T were chosen as they are capable of forming very efficient exciplexes, which serve to help harvest the excitons.[35,36] All layers, except PEDOT:PSS, were thermally evaporated. For a detailed description of the fabrication process, see the Experimental section.

Previous works have reported that the roughness of organic surfaces increases when an ultrathin emissive layer is deposited on top of them.[37] To determine if this also applies to **DMAC-TRZ** ultrathin layers, AFM images were obtained for films of mCP (20 nm)/**DMAC-TRZ** (0 nm, 0.1 nm, 0.3 nm, 1 nm) and are presented in Figure S7. An increase in roughness (S_q) is observed. This indicates that the formation of **DMAC-TRZ** layers occurs through an island growth mode, driven by molecular aggregation. This is further illustrated in Figure S8, which shows a cross-sectional SEM image of a device with a 1 nm-thick EML. From the image it is clear that the mCP and PO-T2T layers are contiguous, which is beneficial for the formation of the exciplexes whose energy is ultimately transferred to the scattered **DMAC-TRZ** molecules for light emission. Therefore, the use of the term "layer" to refer to the scattered emitter molecules might be misleading, and any thickness value associated with them should only be interpreted as a convenient way to quantify the number of molecules deposited estimated from the deposition rate and time.

In general, the optimum thickness for ultrathin emissive layers is a trade-off between concentration quenching (triplet−triplet annihilation grows more prominent as the distance between the emitting molecules becomes shorter) and efficient exciton utilization and energy transfer. As different compounds

https://doi.org/10.1021/acsphotonics.4c01039
ACS Photonics 2024, 11, 4151−4160

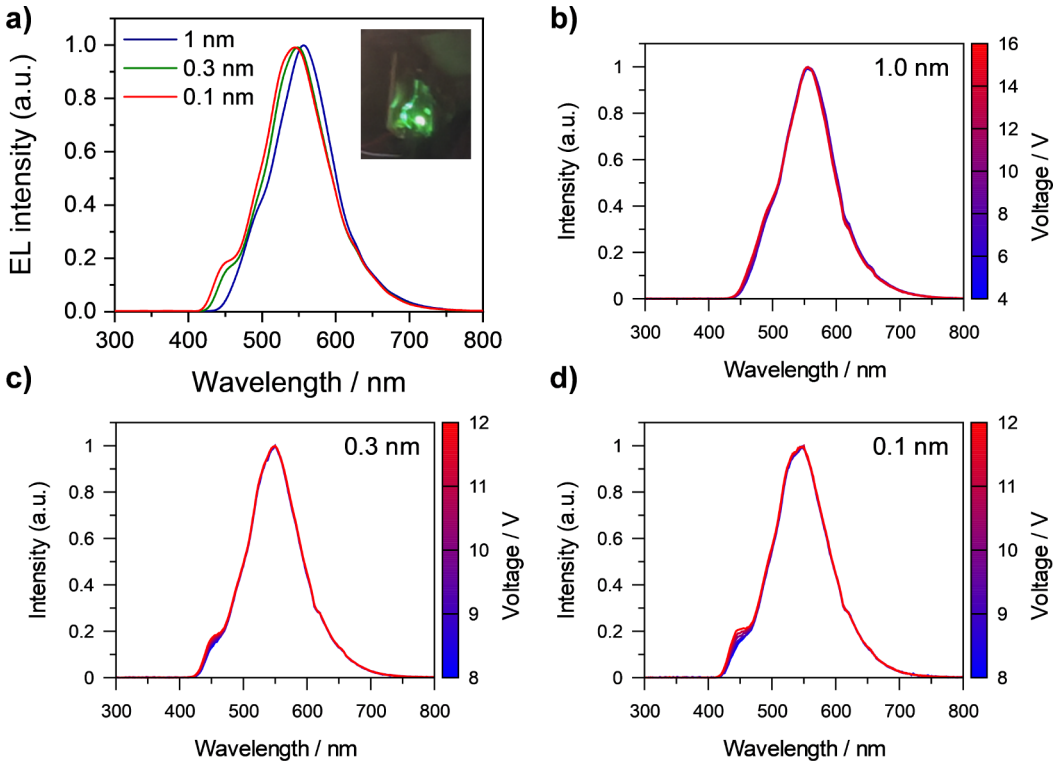

Figure 4. (a) Electroluminescent spectra (at 10.0 V) for devices with different thicknesses (1, 0.3, and 0.1 nm) of the undoped DMAC-TRZ emissive layer (inset: photo of a working device with a 1 nm-thick emissive layer). (b–d) Electroluminescence spectrum versus voltage of devices with different DMAC-TRZ layer thicknesses: 1, 0.3, and 0.1 nm, respectively.

Table 2. Summary of OLED Characteristics for Devices with Different Thicknesses of the Undoped DMAC-TRZ Emissive Layer[a]

DMAC-TRZ layer thickness/nm	EL peak position/nm (CIE xy coordinates)	Turn-on voltage/V	Max. luminance/cd m^{-2} @ Voltage	Max. current efficiency/cd A^{-1} @ Luminance
0.1	544 (0.34, 0.51)	3.9	5209 @11.0 V	20.1 @92.9 cd m^{-2}
0.3	548 (0.35, 0.52)	3.4	8238 @10.6 V	30.8 @135 cd m^{-2}
1	556 (0.38, 0.53)	3.3	11152 @13.4 V	67.6 @19.8 cd m^{-2}

[a]CIE 1931 color points refer to the devices operated at 10.0 V.

have different tendencies to aggregate and susceptibilities to concentration quenching,[16,38,39] it is not guaranteed that the optimum thickness found for one emitter will be suitable for a different molecule. Since the incorporation of an ultrathin emissive layer of **DMAC-TRZ** has never been reported before, it was necessary to explore the performance of various thicknesses of ultrathin **DMAC-TRZ** films. Therefore, three different thicknesses of **DMAC-TRZ** films were assessed in OLEDs, namely 0.1, 0.3, and 1 nm. Their electroluminescent spectral characteristics are illustrated in Figure 4a and summarized in Table 2. All three types of devices showed bright yellowish-green electroluminescence (inset in Figure 4a). Their EL spectra show a peak centered around 550 nm, which indicates prominent emission from the EML molecules despite the significant red-shift compared to the PL spectrum of **DMAC-TRZ** neat films (~50 nm, Figure S2). In fact, this is consistent with the intramolecular charge-transfer (ICT) nature of the electronic transitions in **DMAC-TRZ**,[13] which makes the electronic states of the molecule sensitive to differences in polarity of the surrounding medium.[40] Light interference effects, absent in a neat film, also contribute to modifying the original spectrum in the devices.

In the 0.1 and 0.3 nm ultrathin films a peak shoulder at 450 nm appears, totally absent in the devices with a 1 nm-thick **DMAC-TRZ** film. With the aim of understanding its origin, the electroluminescence spectra of the devices were acquired at different voltage values. While the EL spectrum of the devices with a 1 nm thick layer remains identical independently of the voltage applied to them (Figure 4b), in devices whose EL spectra show a shoulder, its relative intensity (with respect to the main emission peak) grows together with the applied voltage and the luminance (Figure 4c,d). As previously highlighted the subnanometer thickness of the emissive layer is just nominal, meaning that the **DMAC-TRZ** molecules are not in the form of a neat layer. The decrease in nominal thickness from 1 nm to 0.3 or 0.1 nm hence corresponds to fewer and sparser emitter molecules that can be excited, making the saturation of their emission more pronounced, especially at higher voltage (and current) values. As a consequence, recombination in those devices also takes place within other layers. In this case, as the PL peak of the perovskite layer perfectly overlaps with the EL peak shoulder (Figure S3a), we can deduce that for samples with a 0.3 and a 0.1 nm-thick active layer a small but non-negligible part of the radiative recombination of the carriers occurs in the perovskite

https://doi.org/10.1021/acsphotonics.4c01039
ACS Photonics 2024, 11, 4151–4160

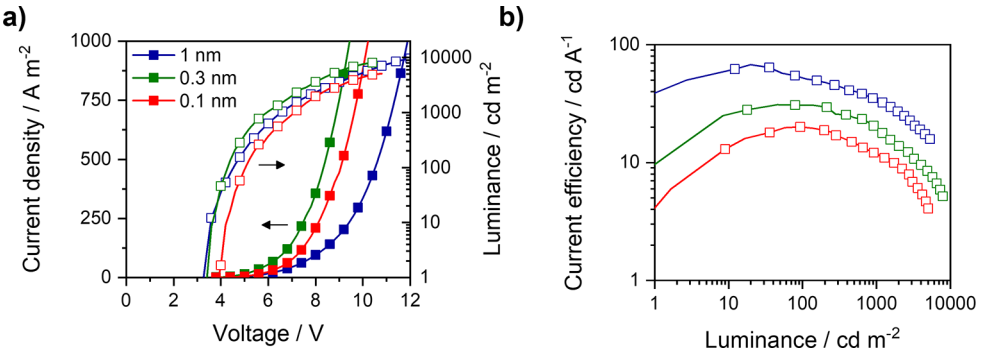

Figure 5. (a) Current density−voltage−luminance (J−V−L) characteristics and (b) current efficiency versus luminance for OLEDs with a m-$CsPbCl_3$ HTL and an ultrathin (1, 0.3, and 0.1 nm) vacuum-processed DMAC-TRZ active layer.

layer. Charge recombination happening throughout different layers negatively affects the color purity of the devices. This is seen in the CIE 1931 color points of the devices with 0.1 and 0.3 nm-thick EMLs, that are not only further away from the curved edge of the gamut (spectral locus, Figure S10) but also move away from it as the luminance increases (Figure S11), mainly due to the decrease of the y-ordinate (Table S1). On the contrary, the devices with a 1 nm-thick EML show a purer, voltage-independent yellowish-green color (CIE 1931 coordinates of 0.38, 0.53 at 10.0 V).

Apart from the color purity, as only a small fraction of charge carriers recombining within the perovskite layer do so radiatively (Figure S3), devices with thinner (0.1 and 0.3 nm thick) EMLs are expected to have lower electroluminescence efficiencies. This is reflected in their J−V−L characteristics (Figure 5a and Table 2). Even if the three types of devices exhibit similar current density versus voltage characteristics, there exist some trending differences dictated by the thickness of the emissive layer. For example, devices have a turn-on voltage that decreases with increasing emitting layer thickness, with values of 3.9 and 3.3 V for 0.1 and 1 nm, respectively. In all cases, however, the J−V characteristics suggest that the perovskite transport layer poses little to no barrier to charge injection. From the moment they turn on, the devices' luminance increases with the voltage at the same pace. At any given voltage, the devices with a lower EML thickness have a higher current density flowing through them. This leakage current that does not translate into a brighter light emission is the cause of their lower EL efficiency values (30.8 cd A^{-1} for the device with a thickness of 0.3 nm and 20.1 cd A^{-1} for the 0.1 nm one). On the other hand, the efficient utilization of excitons in the devices with an EML thickness of 1.0 nm, translated into a maximum current efficiency of 67.6 cd A^{-1}, corresponding to 20.8% EQE_{max} (Figure 5b), and, in general, higher current efficiencies along the entire range of luminance. More importantly, these performances are almost identical to those reported for thick (20 nm) nondoped devices with the same emitter,[13] but were achieved by consuming 20 times less compound. As far as the luminance is concerned, the devices with an EML thickness of 1 nm perform the best, achieving a peak luminance of 11 152 cd m^{-2}, comparable to literature values.[13] Also, the distribution of luminance and EQE obtained from 29 devices showed good reproducibility (Figure S12). In other words, among the thickness values investigated, 1 nm represents the optimal thickness that allows for a reduction in material costs without compromising the efficiency, the luminance, and the color purity, while the perovskite transport layer fulfills the important role of increasing the total device thickness without affecting the performance. While optical and electrical simulations suggest that higher thicknesses might slightly increase the efficiency even further (Figure S13), the expense of higher material consumption might not make it worth it. Finally, the operational lifetime was also measured, showing a LT_{50} (time to reach a luminance that is 50% of the initial one) of 1.72 h at an initial luminance of 60 cd m^{-2} (Figure S14).

CONCLUSIONS

In summary, we demonstrated the use of a thick perovskite ($CsPbCl_3$) hole transport layer in OLEDs with an undoped TADF-based emissive layer, either solution-processed or vacuum-deposited. To do so, we first selected TADF emitters that are lightly susceptible to aggregation-caused quenching, namely **tBuCz2m2pTRZ** and **DMAC-TRZ**. In the first case, we assessed the compatibility of the perovskite HTL with subsequent solvent coating, with no detrimental effect of solution processing over the $CsPbCl_3$ layer. We combined the perovskite HTL with the **tBuCz2m2pTRZ** emitter in OLEDs, with devices that reached a peak luminance of 4660 cd m^{-2} and that could maintain their current efficiency above 15 cd A^{-1} at luminances over 1000 cd m^{-2}. In the case of **DMAC-TRZ**, the emitter was successfully employed in the form of an ultrathin vacuum-deposited layer, an approach that was facilitated by the compensation in thickness provided by the inorganic perovskite layer. The resulting 1 nm emitting layer OLEDs showed a low turn-on voltage of 3.3 V, a high luminance of 11 152 cd m^{-2} and a striking efficiency of 67.6 cd A^{-1}, comparable to that of TADF-OLEDs with thick nondoped emitting layers, but with a 20-fold reduction in materials cost. The ability to produce highly efficient undoped OLEDs using diverse TADF emitters with different fabrication techniques in combination with a perovskite transport layer highlights the versatility of the approach for different device configurations with the advantages of a simple device fabrication and reduced costs.

EXPERIMENTAL SECTION

Materials. Cesium chloride (CsCl, 99.999%) was purchased from Sigma-Aldrich. Aqueous poly(3,4-ethylenedioxythiophene) polystyrenesulfonate (PEDOT:PSS) dispersion was obtained from Clevios (P VP AI 4083 or P VP CH 8000). Organic materials (1,3-bis(N-carbazolyl)benzene (mCP), 10-(4-(4,6-Diphenyl-1,3,5-triazin-2-yl)phenyl)-9,9-dimethyl-9,10-dihydroacridine (DMAC-TRZ) and 2,4,6-tris[3-

https://doi.org/10.1021/acsphotonics.4c01039
ACS Photonics 2024, 11, 4151−4160

(diphenylphosphinyl)phenyl]-1,3,5-triazine (PO-T2T) and lead chloride ($PbCl_2$, 99.999%) were purchased from Lumtec. tBuCz2m2pTRZ was synthesized according to a previous report.[12] All the reagents except for PEDOT:PSS were stored under N_2 filled atmosphere.

Sample and Device Preparation. Prepatterned 150 nm thick indium tin oxide (ITO)-coated glass plates (3 cm × 3 cm) were used as transparent conductive substrates. They were subsequently cleaned ultrasonically in tap water-detergent, deionized water, and 2-propanol baths for 5 min. After drying, the substrates were placed in a UV−ozone cleaner (Jelight 42−220) for 15 min. The ITO substrates were coated with PEDOT:PSS solution (2000 rpm for 60 s for P VP AI 4083, resulting in 30 nm, or 2000 rpm for 60 s for a P VP CH 8000 suspension diluted 2.3 times with distilled water, resulting in 40 nm. The thickness of the PEDOT:PSS layers was determined with an Ambios XP-1 profilometer). The PEDOT:PSS films were thermally treated at 150 °C for 10 min. These substrates were transferred to the vacuum chamber, where $CsPbCl_3$, mCP, DMAC-TRZ, PO-T2T, Ba and Ag were thermally deposited. A 10 mg mL^{-1} dendrimer (tBuCz2m2pTRZ) in chlorobenzene solution was spin-coated at 1500 rpm for 60 s to form a 40 nm-thick EML, which was then annealed at 120 °C for 10 min. PO-T2T, Ba and Ag for the tBuCz2m2pTRZ were thermally deposited. Layers referred to as m-$CsPbCl_3$ included 2 nm CsCl interlayers before and after the $CsPbCl_3$ layer. The perovskite HTLs were thermally annealed at 120 °C for 10 min before the deposition of the subsequent layers. The vacuum evaporation rates were 0.135 nm s^{-1}, 0.06 nm s^{-1}, 0.001 nm s^{-1}, 0.1 nm s^{-1} and 0.05 nm s^{-1} for the perovskite, HTL, EL, ETL and cathode, respectively, with the background pressure being around 3×10^{-6} bar. The deposition rates were measured using calibrated quartz crystal microbalances (QCM, with an Inficon SQC-310 deposition controller to monitor their frequency) placed inside of the evaporation chamber, next to the crucibles. The tooling of the emitting materials was performed by depositing a film on a cleaned glass substrate and comparing the film thickness estimated from the signal of the QCM balance to the value measured with a profilometer (Ambios XP-1). The amount of material deposited in the ultrathin emitting layers was estimated from the deposition rate and the deposition time and is given as a nominal layer thickness in nm. Shadow masks were used during the metal evaporation to obtain a final active area of 6 mm^2. Devices were not exposed to water vapor or O_2 after the cathode deposition and before the characterization.

Solvent Treatment of Perovskite Film. To reproduce the exact conditions that would be used during device fabrication, the thick perovskite films were deposited on top of a PEDOT:PSS CH8000 layer. Then, 100 μL of pure solvent were spin-coated onto the film at 1500 rpm for 60 s. The films were annealed at 120 °C for 10 min after the solvent treatment. The thickness of the stack was measured before and after the treatment with an Ambios XP-1 profilometer and the surface roughness was measured by means of AFM.

X-ray Diffraction. The crystalline structure of the perovskite film was studied by XRD. The patterns were collected in Bragg−Brentano geometry on an Empyrean PANalytical powder diffractometer with a copper anode operated at 45 kV and 40 mA and then analyzed with High Score software.

Grazing-Incidence Wide-Angle X-ray Scattering. GIWAXS patterns were measured using a customized setup equipped with a laboratory MetalJet X-ray source (Excillum) with an X-ray energy of 9.25 keV (λ = 1.34 Å). The X-ray incidence angle was set to ∼0.5°. Samples were measured in a vacuum. The GIWAXS patterns were acquired by a two-dimensional detector (Pilatus 300 K, Dectris, Switzerland, pixel size 175 × 175 μm) with a sample-to-detector distance of ∼114 mm and integration time of 600 s.

Atomic Force Microscopy and Scanning Electron Microscopy. AFM measurements were performed with a Bruker MultiMode 8 AFM equipped with a NanoScope V AFM controller. Images were acquired in tapping mode using silicon tips with a natural resonance frequency of 300 kHz and with an equivalent constant force of 40 N m^{-1}. The scan rate was adjusted during the scanning of each image (0.1−1 Hz, 256−512 samples/line). Images were treated with Gwyddion SPM data analysis software. For the scanning electron microscopy (SEM) images of the tBuCz2m2pTRZ and DMAC-TRZ devices, a glass substrate fully covered with a 35 nm-thick ITO layer was used for the subsequent patternless deposition of the PEDOT:PSS CH8000, m-$CsPbCl_3$, tBuCz2m2pTRZ or mCP and DMAC-TRZ, PO-T2T, Ba and Ag layers with respective thicknesses of 40, 100, 40, or 20 and 1, 40 or 60, 5, and 70 nm, with the same modalities used for the working devices. Then, the stacks were snapped in half and the SEM images were acquired with a Hitachi S8010 ultra high-resolution scanning electron microscope (Hitachi High-Tech Corporation).

Photophysical Measurements. The photoluminescence spectra were measured with an Avantes AvaSpec-2048L spectrometer equipped with a diode laser of integrated optics, with an emission wavelength of 375 nm. The PL quantum yield was measured with a Hamamatsu C9920−02 Absolute PL quantum yield spectrometer equipped with a A10094 integrating sphere unit, a A10080−02 monochromator, a Xe/Hg−Xe lamp and a PMA-12 photonic multichannel analyzer. The wavelength used for excitation was 365 nm. The data was analyzed with the U6039−05 PLQY measurement software.

OLEDs Characterization. After full device fabrication, the samples were introduced into a custom setup for a current density and luminance versus voltage ($J-V-L$) scan. For this we employed a Keithley 2400 Source-Meter and a photodiode coupled to a Keithley 6485 picoammeter. A LabVIEW program was used to control the Keithleys and to obtain the data. The photodiode was calibrated using a Konica Minolta LS-150 equipped with a 110 close-up lens for the measurement of small areas and controlled through the CS-S20 Data Management Software. The electroluminescence spectra were measured with an Avantes AvaSpec-2048L spectrometer.

Optical and Electrical Simulations. The current, recombination and outcoupling efficiencies for the devices were obtained by simulating the full device stack with the software Setfos 5.4 (Fluxim). The devices architecture was modeled with mobilities and energy levels values from literature. For the modeling of the perovskite transport layer mobile ions were introduced and their effect on the injection into the layer was modeled as a change of its energy levels. Experimental data of devices with a 1 nm-thick EML was used as a reference in this stage until good agreement was reached. The presence of traps was also simulated by considering a simplified SRH recombination mechanism in addition to Langevin recombination.

https://doi.org/10.1021/acsphotonics.4c01039
ACS Photonics 2024, 11, 4151−4160

■ ASSOCIATED CONTENT

Supporting Information

The Supporting Information is available free of charge at https://pubs.acs.org/doi/10.1021/acsphotonics.4c01039.

Definition of root-mean-square roughness, chemical structure of the emitters, fluorescence spectrum of DMAC-TRZ neat films, optical properties and XRD patterns of $CsPbCl_3$ films, absorption, photoluminescence, and XRD patterns of m-$CsPbCl_3$ films, GIWAXS extended information, energy level diagrams, CIE 1931 Chromacity Diagrams, AFM images of the ultrathin layers, histograms for device performance statistics, devices electrical simulations, devices lifetime (PDF)

■ AUTHOR INFORMATION

Corresponding Author

Daniel Tordera − *Instituto de Ciencia Molecular (ICMol), Universidad de Valencia, Paterna 46980, Spain;* orcid.org/0000-0001-9283-8801; Email: daniel.tordera@uv.es

Authors

Michele Forzatti − *Instituto de Ciencia Molecular (ICMol), Universidad de Valencia, Paterna 46980, Spain;* orcid.org/0000-0001-8527-2280

Vladimir Held − *Instituto de Ciencia Molecular (ICMol), Universidad de Valencia, Paterna 46980, Spain*

Edoardo Stanzani − *Fluxim AG, Winterthur 8400, Switzerland*

David Hall − *Organic Semiconductor Centre, EaStCHEM School of Chemistry, University of St Andrews, St Andrews KY16 9ST, UK*

Dianming Sun − *Organic Semiconductor Centre, EaStCHEM School of Chemistry, University of St Andrews, St Andrews KY16 9ST, UK*

M. Angeles Hernández-Fenollosa − *Instituto de Tecnología de Materiales, Universitat Politècnica de Valencia, Valencia 46022, Spain*

Isaac Brotons-Alcázar − *Instituto de Ciencia Molecular (ICMol), Universidad de Valencia, Paterna 46980, Spain;* orcid.org/0000-0002-1787-3348

Peter Siffalovic − *CEMEA, Slovak Academy of Sciences, Bratislava 84511, Slovakia;* orcid.org/0000-0002-9807-0810

Sandra Jenatsch − *Fluxim AG, Winterthur 8400, Switzerland;* orcid.org/0000-0003-1311-9898

Eli Zysman-Colman − *Organic Semiconductor Centre, EaStCHEM School of Chemistry, University of St Andrews, St Andrews KY16 9ST, UK;* orcid.org/0000-0001-7183-6022

Henk J. Bolink − *Instituto de Ciencia Molecular (ICMol), Universidad de Valencia, Paterna 46980, Spain;* orcid.org/0000-0001-9784-6253

Complete contact information is available at: https://pubs.acs.org/10.1021/acsphotonics.4c01039

Funding

The authors thank K.P.S. Zanoni for acquiring AFM images. This project has been partly funded by the European Union Horizon 2021 research and innovation program under grant agreement No. 101073045 (TADFsolutions) and the EPSRC grant EP/X026175/1. H.B. acknowledges financial support of the European Research Council (ERC) under the European Union's Horizon 2020 research and innovation program (Grant Agreement No. 834431).

Notes

The authors declare no competing financial interest.

■ REFERENCES

(1) Tang, C. W.; VanSlyke, S. A. Organic Electroluminescent Diodes. *Appl. Phys. Lett.* **1987**, *51* (12), 913−915.

(2) Zou, S.-J.; Shen, Y.; Xie, F.-M.; Chen, J.-D.; Li, Y.-Q.; Tang, J.-X. Recent Advances in Organic Light-Emitting Diodes: Toward Smart Lighting and Displays. *Mater. Chem. Front.* **2020**, *4* (3), 788−820.

(3) Shi, Y.-Z.; Wu, H.; Wang, K.; Yu, J.; Ou, X.-M.; Zhang, X.-H. Recent Progress in Thermally Activated Delayed Fluorescence Emitters for Nondoped Organic Light-Emitting Diodes. *Chem. Sci.* **2022**, *13* (13), 3625−3651.

(4) Goushi, K.; Yoshida, K.; Sato, K.; Adachi, C. Organic Light-Emitting Diodes Employing Efficient Reverse Intersystem Crossing for Triplet-to-Singlet State Conversion. *Nat. Photonics* **2012**, *6* (4), 253−258.

(5) Zhang, Q.; Li, B.; Huang, S.; Nomura, H.; Tanaka, H.; Adachi, C. Efficient Blue Organic Light-Emitting Diodes Employing Thermally Activated Delayed Fluorescence. *Nat. Photonics* **2014**, *8* (4), 326−332.

(6) Chan, C.-Y.; Tanaka, M.; Lee, Y.-T.; Wong, Y.-W.; Nakanotani, H.; Hatakeyama, T.; Adachi, C. Stable Pure-Blue Hyperfluorescence Organic Light-Emitting Diodes with High-Efficiency and Narrow Emission. *Nat. Photonics* **2021**, *15* (3), 203−207.

(7) Lee, D. R.; Kim, B. S.; Lee, C. W.; Im, Y.; Yook, K. S.; Hwang, S.-H.; Lee, J. Y. Above 30% External Quantum Efficiency in Green Delayed Fluorescent Organic Light-Emitting Diodes. *ACS Appl. Mater. Interfaces* **2015**, *7* (18), 9625−9629.

(8) Karthik, D.; Jung, Y. H.; Lee, H.; Hwang, S.; Seo, B.-M.; Kim, J.-Y.; Han, C. W.; Kwon, J. H. Acceptor−Donor−Acceptor-Type Orange−Red Thermally Activated Delayed Fluorescence Materials Realizing External Quantum Efficiency Over 30% with Low Efficiency Roll-Off. *Adv. Mater.* **2021**, *33* (18), 2007724.

(9) Ma, M.; Li, J.; Liu, D.; Mei, Y.; Dong, R. Rational Utilization of Intramolecular Hydrogen Bonds to Achieve Blue TADF with EQEs of Nearly 30% and Single Emissive Layer All-TADF WOLED. *ACS Appl. Mater. Interfaces* **2021**, *13* (37), 44615−44627.

(10) Chen, J.-X.; Wang, K.; Xiao, Y.-F.; Cao, C.; Tan, J.-H.; Wang, H.; Fan, X.-C.; Yu, J.; Geng, F.-X.; Zhang, X.-H.; Lee, C.-S. Thermally Activated Delayed Fluorescence Warm White Organic Light Emitting Devices with External Quantum Efficiencies Over 30%. *Adv. Funct. Mater.* **2021**, *31* (31), 2101647.

(11) Sachnik, O.; Ie, Y.; Ando, N.; Tan, X.; Blom, P. W. M.; Wetzelaer, G.-J. A. H. Single-Layer Organic Light-Emitting Diode with Trap-Free Host Beats Power Efficiency and Lifetime of Multilayer Devices. *Adv. Mater.* **2024**, *36* (16), 2311892.

(12) Sun, D.; Duda, E.; Fan, X.; Saxena, R.; Zhang, M.; Bagnich, S.; Zhang, X.; Köhler, A.; Zysman-Colman, E. Thermally Activated Delayed Fluorescent Dendrimers That Underpin High-Efficiency Host-Free Solution-Processed Organic Light-Emitting Diodes. *Adv. Mater.* **2022**, *34* (23), 2110344.

(13) Tsai, W.-L.; Huang, M.-H.; Lee, W.-K.; Hsu, Y.-J.; Pan, K.-C.; Huang, Y.-H.; Ting, H.-C.; Sarma, M.; Ho, Y.-Y.; Hu, H.-C.; Chen, C.-C.; Lee, M.-T.; Wong, K.-T.; Wu, C.-C. A Versatile Thermally Activated Delayed Fluorescence Emitter for Both Highly Efficient Doped and Non-Doped Organic Light Emitting Devices. *Chem. Commun.* **2015**, *51* (71), 13662−13665.

(14) Wu, S.; Li, S.; Sun, Q.; Huang, C.; Fung, M.-K. Highly Efficient White Organic Light-Emitting Diodes with Ultrathin Emissive Layers and a Spacer-Free Structure. *Sci. Rep.* **2016**, *6* (1), 25821.

(15) Miao, Y.; Yin, M. Recent Progress on Organic Light-Emitting Diodes with Phosphorescent Ultrathin (<1nm) Light-Emitting Layers. *iScience* **2022**, *25* (2), 103804.

(16) Zhao, Y.; Chen, J.; Ma, D. Ultrathin Nondoped Emissive Layers for Efficient and Simple Monochrome and White Organic Light-Emitting Diodes. *ACS Appl. Mater. Interfaces* **2013**, *5* (3), 965−971.
(17) Nanda, G. P.; Sk, B.; Yadav, N.; Rajamanickam, S.; Deori, U.; Mahashaya, R.; Zysman-Colman, E.; Rajamalli, P. Ultrathin Non-Doped Thermally Activated Delayed Fluorescence Emitting Layer for Highly Efficient OLEDs. *Chem. Commun.* **2021**, *57* (100), 13728−13731.
(18) Yamamori, A.; Adachi, C.; Koyama, T.; Taniguchi, Y. Doped Organic Light Emitting Diodes Having a 650-Nm-Thick Hole Transport Layer. *Appl. Phys. Lett.* **1998**, *72* (17), 2147−2149.
(19) Matsushima, T.; Bencheikh, F.; Komino, T.; Leyden, M. R.; Sandanayaka, A. S. D.; Qin, C.; Adachi, C. High Performance from Extraordinarily Thick Organic Light-Emitting Diodes. *Nature* **2019**, *572* (7770), 502−506.
(20) Kang, D.-H.; Kim, S.-G.; Kim, Y. C.; Han, I. T.; Jang, H. J.; Lee, J. Y.; Park, N.-G. CsPbBr3/CH3NH3PbCl3 Double Layer Enhances Efficiency and Lifetime of Perovskite Light-Emitting Diodes. *ACS Energy Lett.* **2020**, *5* (7), 2191−2199.
(21) Khan, R.; Chu, S.; Li, Z.; Ighodalo, K. O.; Chen, W.; Xiao, Z. High Radiance of Perovskite Light-Emitting Diodes Enabled by Perovskite Heterojunctions. *Adv. Funct. Mater.* **2022**, *32* (32), 2203650.
(22) Baranowski, M.; Plochocka, P.; Su, R.; Legrand, L.; Barisien, T.; Bernardot, F.; Xiong, Q.; Testelin, C.; Chamarro, M. Exciton Binding Energy and Effective Mass of CsPbCl 3: A Magneto-Optical Study. *Photonics Res.* **2020**, *8* (10), A50.
(23) Chin, S.-H.; Mardegan, L.; Palazon, F.; Sessolo, M.; Bolink, H. J. Dimensionality Controls Anion Intermixing in Electroluminescent Perovskite Heterojunctions. *ACS Photonics* **2022**, *9* (7), 2483−2488.
(24) El Ajjouri, Y.; Palazon, F.; Sessolo, M.; Bolink, H. J. Single-Source Vacuum Deposition of Mechanosynthesized Inorganic Halide Perovskites. *Chem. Mater.* **2018**, *30* (21), 7423−7427.
(25) Ullah, S.; Yang, P.; Li, Y.; Wang, J.; Liu, L.; Mahmood, R.; Yang, S.-E.; Xia, T.; Guo, H.; Chen, Y. Two Step Vapor-Processing and Experimental Investigations of All-Inorganic CsPbCl3 Perovskite Films for Optoelectronic Applications. *Mater. Lett.* **2021**, *294*, 129819.
(26) Rodkey, N.; Kaal, S.; Sebastia-Luna, P.; Birkhölzer, Y. A.; Ledinsky, M.; Palazon, F.; Bolink, H. J.; Morales-Masis, M. Pulsed Laser Deposition of Cs2AgBiBr6: From Mechanochemically Synthesized Powders to Dry, Single-Step Deposition. *Chem. Mater.* **2021**, *33* (18), 7417−7422.
(27) Ishii, A.; Miyasaka, T. Sensitized Yb3+ Luminescence in CsPbCl3 Film for Highly Efficient Near-Infrared Light-Emitting Diodes. *Adv. Sci.* **2020**, *7* (4), 1903142.
(28) Kaji, H.; Suzuki, H.; Fukushima, T.; Shizu, K.; Suzuki, K.; Kubo, S.; Komino, T.; Oiwa, H.; Suzuki, F.; Wakamiya, A.; Murata, Y.; Adachi, C. Purely Organic Electroluminescent Material Realizing 100% Conversion from Electricity to Light. *Nat. Commun.* **2015**, *6* (1), 8476.
(29) Liao, Y.; Tian, N.; Wang, J.; Yao, D.; Zheng, G.; Zhou, B.; Yang, Y.; Long, F. Performance Enhancement of Evaporated CsPbI2Br Perovskite Solar Cells with a CuSCN Hole Transport Layer via a Cesium Bromide Buffer Layer. *ACS Appl. Energy Mater.* **2022**, *5* (8), 9542−9548.
(30) Tian, Y.; Ling, Y.; Shu, Y.; Zhou, C.; Besara, T.; Siegrist, T.; Gao, H.; Ma, B. A Solution-Processed Organometal Halide Perovskite Hole Transport Layer for Highly Efficient Organic Light-Emitting Diodes. *Adv. Electron. Mater.* **2016**, *2* (7), 1600165.
(31) Bartels, W. J. Characterization of Thin Layers on Perfect Crystals with a Multipurpose High Resolution X-ray Diffractometer. *J. Vac. Sci. Technol. B Microelectron. Process. Phenom.* **1983**, *1* (2), 338−345.
(32) Yadav, R. A. K.; Dubey, D. K.; Chen, S.-Z.; Liang, T.-W.; Jou, J.-H. Role of Molecular Orbital Energy Levels in OLED Performance. *Sci. Rep.* **2020**, *10* (1), 9915.
(33) Dong, J.; Song, D.; Meng, J.; Lu, Y.; Li, Y.; Qiao, B.; Zhao, S.; Xu, Z. Interface Energy Level Alignment and Improved Film Quality with a Hydrophilic Polymer Interlayer to Improve the Device Efficiency and Stability of All-Inorganic Halide Perovskite Light-Emitting Diodes. *J. Mater. Chem. C* **2020**, *8* (20), 6743−6748.
(34) Kim, Y.-H.; Cho, H.; Heo, J. H.; Kim, T.-S.; Myoung, N.; Lee, C.-L.; Im, S. H.; Lee, T.-W. Multicolored Organic/Inorganic Hybrid Perovskite Light-Emitting Diodes. *Adv. Mater.* **2015**, *27* (7), 1248−1254.
(35) Hung, W.-Y.; Fang, G.-C.; Chang, Y.-C.; Kuo, T.-Y.; Chou, P.-T.; Lin, S.-W.; Wong, K.-T. Highly Efficient Bilayer Interface Exciplex For Yellow Organic Light-Emitting Diode. *ACS Appl. Mater. Interfaces* **2013**, *5* (15), 6826−6831.
(36) Lee, J.-H.; Cheng, S.-H.; Yoo, S.-J.; Shin, H.; Chang, J.-H.; Wu, C.-I.; Wong, K.-T.; Kim, J.-J. An Exciplex Forming Host for Highly Efficient Blue Organic Light Emitting Diodes with Low Driving Voltage. *Adv. Funct. Mater.* **2015**, *25* (3), 361−366.
(37) Zhao, C.; Zhang, T.; Chen, J.; Yan, D.; Ma, D. High-Performance Hybrid White Organic Light-Emitting Diodes with Simple Emitting Structures and Low Efficiency Roll-off Based on Blue Thermally Activated Delayed Fluorescence Emitters with Bipolar Transport Characteristics. *J. Mater. Chem. C* **2018**, *6* (35), 9510−9516.
(38) Wu, T.-L.; Lei, J.; Hsieh, C.-M.; Chen, Y.-K.; Huang, P.-Y.; Lai, P.-T.; Chou, T.-Y.; Lin, W.-C.; Chen, W.; Yu, C.-H.; Hsu, L.-Y.; Lin, H.-W.; Cheng, C.-H. Substituent Engineering of the Diboron Molecular Architecture for a Nondoped and Ultrathin Emitting Layer. *Chem. Sci.* **2022**, *13* (44), 12996−13005.
(39) Dai, X.; Yao, F.; Li, J.; Yu, H.; Cao, J. Color-Stable Non-Doped White Phosphorescent Organic Light-Emitting Diodes Based on Ultrathin Emissive Layers. *J. Phys. Appl. Phys.* **2020**, *53* (5), 055106.
(40) Kahle, F.-J.; Rudnick, A.; Bässler, H.; Köhler, A. How to Interpret Absorption and Fluorescence Spectra of Charge Transfer States in an Organic Solar Cell. *Mater. Horiz.* **2018**, *5* (5), 837−848.

https://doi.org/10.1021/acsphotonics.4c01039
ACS Photonics 2024, 11, 4151−4160